

Dielectric loss in epitaxial Al/GaAs/Al trilayers for superconducting circuitsC.R.H. McRae,^{1,2, a)} A. McFadden,³ R. Zhao,^{1,2} H. Wang,^{1,2} J.L. Long,^{1,2} T. Zhao,^{1,2} S. Park,^{1,2} M. Bal,^{1,2} C.J. Palmstrm,^{3,4} and D.P. Pappas²¹⁾*Department of Physics, University of Colorado, Boulder, Colorado 80309*²⁾*National Institute of Standards and Technology, Boulder, Colorado 80305*³⁾*Department of Electrical and Computer Engineering, University of California, Santa Barbara, CA 93106*⁴⁾*Materials Department, University of California, Santa Barbara, CA 93106*

(Dated: 23 September 2020)

Epitaxially-grown superconductor/dielectric/superconductor trilayers have the potential to form high-performance superconducting quantum devices and may even allow scalable superconducting quantum computing with low-surface-area qubits such as the merged-element transmon. In this work, we measure the power-independent loss and two-level-state (TLS) loss of epitaxial, wafer-bonded, and substrate-removed Al/GaAs/Al trilayers by measuring lumped element superconducting microwave resonators at millikelvin temperatures and down to single photon powers. The power-independent loss of the device is $(4.8 \pm 0.1) \times 10^{-5}$ and resonator-induced intrinsic TLS loss is $(6.4 \pm 0.2) \times 10^{-5}$. Dielectric loss extraction is used to determine a lower bound of the intrinsic TLS loss of the trilayer of 7.2×10^{-5} . The unusually high power-independent loss is attributed to GaAs's intrinsic piezoelectricity.

Keywords: superconducting quantum computing, TLS loss, resonator, gallium arsenide, piezoelectricity

I. INTRODUCTION

The investigation of the electrical properties of dielectric materials and interfaces in the millikelvin-temperature and single-photon-power regime is a burgeoning field in superconducting microwave circuits and is critical to performance enhancement in superconducting quantum computing.¹ In particular, epitaxially-grown dielectrics are of interest because crystalline materials with low defect density have the potential to exhibit lower two-level-system (TLS) loss,^{2,3} the dominant form of loss in high performance superconducting quantum circuits.^{1,4} In addition, the ultra-high vacuum environment used in epitaxial growth allows for lower TLS loss attributed to cleaner interfaces between materials.^{5,6}

The discovery of a low-loss superconductor/dielectric/superconductor trilayer would allow the implementation of scalable, high-performance quantum computing designs such as the merged-element transmon.⁷

Because the epitaxial growth of GaAs and Al/GaAs heterostructures is well-established,^{8–11} GaAs is a natural candidate for epitaxial growth for superconducting quantum devices.

In this work, we measure the power-independent loss and TLS loss of epi-Al/GaAs/Al trilayers on Al₂O₃ made using a wafer bonding technique.¹² To determine this loss, we perform cryogenic microwave measurements of lumped element superconducting microwave resonators with parallel plate capacitors formed from these trilayers. We demonstrate that these epitaxial films perform similarly to bulk GaAs¹³ and exhibit loss dominated by power-independent loss which we attribute to the intrinsic piezoelectricity of GaAs.

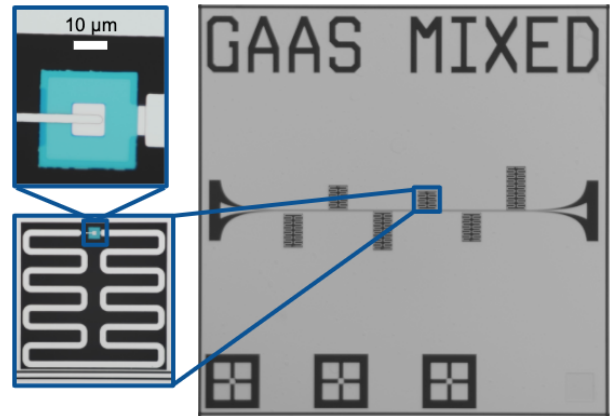


FIG. 1. Optical micrographs of a lumped element resonator with a Al/GaAs/Al parallel plate capacitor and liftoff Al inductor. Blue region is GaAs, light grey is Al, and dark grey is sapphire substrate. Blue squares show a zoom-in of the trilayer resonator with an inductor design of $N = 7$ (seven inductor meanders). Chip shown is sample Trilayer 1, with a zoom-in of device A, as in Table I.

II. DEVICE DESIGN AND FABRICATION

The material under test is a 40 nm epi-Al/40 nm epi-GaAs/40 nm epi-Al trilayer with a 20 nm atomic-layer-deposited (ALD) Al₂O₃ bonding layer, bonded to an Al₂O₃(0001) substrate. The interfaces are abrupt and epitaxial, and the GaAs is single crystalline as determined by transmission electron microscopy.¹² More details on the growth, wafer bonding, substrate removal, and regrowth processes, as well as materials imaging and characterization, can be found in Ref. 12. Trilayer lumped element resonators (shown in Fig. 1) are patterned using a six-step lithography and etch process (Fig. 2). First, the top capacitor plate is defined us-

^{a)}Electronic mail: corey.rae.mcr@colorado.edu

TABLE I. Parameters extracted from cryogenic microwave measurements of lumped element resonators with Al/GaAs/Al parallel plate capacitors (Trilayer) and interdigitated capacitors (Planar). All measurements were performed in DR1 unless stated otherwise. Values are given with their 95% confidence intervals where available. N : number of inductor meanders. f_0 : resonance frequency. $1/Q_{i,HP}$: inverse high power internal quality factor. $F\delta_{\text{TLS}}^0$: resonator-induced intrinsic TLS loss. $1/Q_{i,LP}$: inverse low power internal quality factor. This value is reported if $F\delta_{\text{TLS}}^0$ is unavailable. $1/Q_c$: inverse coupling quality factor.

Device Label	Sample	N	f_0 (GHz)	$1/Q_{i,HP}$ ($\times 10^{-6}$)	$F\delta_{\text{TLS}}^0$ ($\times 10^{-6}$)	$1/Q_{i,LP}$ ($\times 10^{-6}$)	$1/Q_c$ ($\times 10^{-6}$)
A	Trilayer 1	7	7.41	48 ± 1	64 ± 2	-	15.3
B	Planar 1	7	7.92	0.3 ± 0.1	6.2 ± 0.2	-	2.6
-	Trilayer 1 DR2	17	4.79	57.8	~ 18.3	-	23.6
-	Trilayer 1	9	6.39	108	-	~ 217	17
-	Trilayer 2	7	7.41	92.6	-	~ 110	163

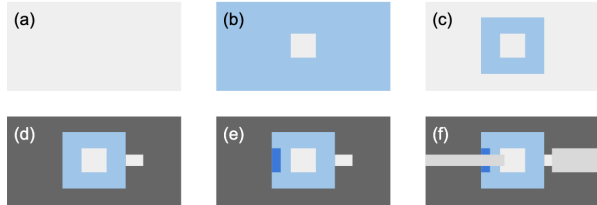


FIG. 2. Diagram of fabrication process for epi-Al/GaAs/Al trilayer lumped element resonators. (a) shows trilayer prior to processing. Fabrication steps shown are (b) capacitor top plate definition, (c) GaAs layer etch, (d) bottom Al layer etch, (e) undercut, and (f) Al liftoff. Al is shown as light grey, GaAs is light blue, undercut GaAs is darker blue, and Al_2O_3 substrate is dark grey.

ing Megaposit MF26A developer¹⁴ to etch the top layer of Al (Fig. 2 (b)). Then, the GaAs is etched away with Transene GA300 wet etchant heated to 33 °C (Fig. 2 (c)). A second MF26A etch is used to remove the next layer of Al as well as the AlO_x bonding layer (Fig. 2 (d)). An undercut of the bottom capacitor plate is performed with Transene D Al Etchant (Fig. 2 (e)). Transene A Al Etchant is used to fully remove residual Al in large blank areas. Finally, a liftoff process of e-beam deposited Al is used to form the feedline and inductors (Fig. 2 (f)). Auto-spun Megaposit SPR660 photoresist exposed using a maskless aligner is used for lithography in all but the liftoff step, where a trilayer of MicroChem PMMA A2, MicroChem LOR5A, and SPR660 are used. An oxygen plasma ash is used to prepare the surface prior to Al deposition.

The trilayer resonator design is similar to that in Ref. 15. The parallel plate capacitor is designed to have a $10 \mu\text{m} \times 10 \mu\text{m}$ top plate and is connected to each end of the inductor by liftoff. The inductor is $15 \mu\text{m}$ in width with a gap between inductive meanders of $30 \mu\text{m}$ and inductor length varies by varying the number of meanders N between 7 and 17, corresponding to resonance frequencies f_0 between 4.7 and 7.5 GHz. Coupling quality factors vary between roughly 10,000 and 100,000 in order to facilitate critical coupling.

About 17% of the total Al top electrode area is liftoff Al, not epi-Al. This could obscure the epi-Al/GaAs/Al loss if trilayer loss is much lower than liftoff interface loss. In future experiments, this liftoff area should be replaced

by an airbridge.

In order to take into account the effect of the inductor circuit element, trilayer resonator measurements are compared to those of planar resonators, for which the same inductor design is used but the trilayer is replaced by an interdigitated capacitor. Planar resonators are fabricated using liftoff e-beam Al on sapphire to imitate the inductor fabrication in the trilayer devices.

III. MICROWAVE MEASUREMENTS AND LOSS EXTRACTION

Samples are clamped into sample boxes made from gold-plated oxygen-free high thermal conductivity copper, with wirebonds used for electrical connection. Measurements are performed in two different cryogen-free dilution refrigerators (DRs): DR1, at a temperature of 12 mK, and DR2, at a temperature below 10 mK. Applied power is varied between -5 and -90 dBm with roughly 70 dB of line attenuation.

Internal quality factors Q_i , coupling quality factors Q_c , and resonance frequencies f_0 are determined by way of a fitting routine that implements the diameter correction method,¹⁷ with a fixed- f_0 Monte Carlo fit, ten points on either side of the resonance frequency used for normalization, and one 3-dB bandwidth of data around the resonance used for the fitting itself. Resonator data, as well as measurement and fitting codes, can be found online.¹⁸

Four trilayer resonators and one planar resonator were successfully measured, as shown in Table I, and two were able to be fitted at sufficiently high and low powers as to allow TLS model fitting.¹⁶ These two devices are labeled device A (trilayer resonator) and device B (planar resonator). Measurements of the other trilayer resonators in Table I support the values seen in the measurements of device A.

Fig. 3 shows power sweeps of loss δ for resonators A and B as well as fits to the TLS model, whose results are reported in Table I. Time-averaged number of photons in the resonator $\langle n_{\text{ph}} \rangle$ is estimated using the resonator Q_c , Q_i , and f_0 , and total power, as in Ref. 19, and critical number of photons n_c is a fitting parameter in the TLS model.¹⁶

At high power, the loss of trilayer resonator A is $(4.8 \pm 0.1) \times 10^{-5}$, close to the resonator-induced intrinsic TLS loss, $(6.4 \pm 0.2) \times 10^{-5}$. This loss is with a factor of 3 of

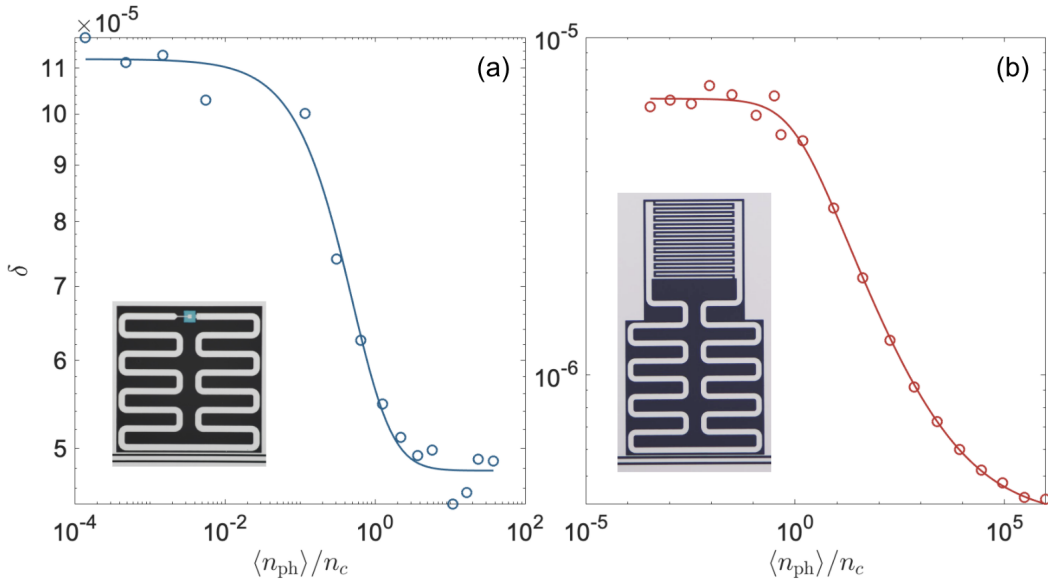


FIG. 3. Loss δ as a function of normalized number of photons in the resonator $\langle n_{\text{ph}} \rangle / n_c$ at $T \sim 12$ mK for resonators (a) A and (b) B, defined in Table I. Data is denoted as circles, and fitting to the TLS model¹⁶ is denoted as a solid line. Insets show representations of the measured devices.

the piezoelectric loss measured in bulk GaAs,¹³ and thus we attribute this loss to piezoelectricity as well.

We can determine a lower bound for the intrinsic TLS loss of the Al/GaAs/Al trilayer, independent of the effect of the resonator wiring, by implementing a modified version of dielectric loss extraction.¹⁵ The resonator-induced intrinsic TLS loss in device A, $\delta_A = F_A \delta_{\text{TLS},A}^0$, where F_A is the filling factor of the TLS material in device A, is a weighted sum of intrinsic TLS loss in the planar inductor δ_L and the Al/GaAs/Al trilayer capacitor $\delta_{\text{Al/GaAs/Al}}$, as:

$$\delta_A = \frac{C_L}{C_{\text{tot}}} \delta_L + \frac{C_C}{C_{\text{tot}}} \delta_{\text{Al/GaAs/Al}}, \quad (1)$$

where C_L (C_C) is the capacitance of the inductor (capacitor) circuit component, and total capacitance is $C_{\text{tot}} = C_L + C_C$. If we assume all TLS loss in planar resonator B is from the inductor, which is identical in design to the inductor in device A, then $\delta_B = \delta_L$. We can then determine a lower bound on the loss of the epitaxial Al/GaAs/Al trilayer by

$$\delta_{\text{Al/GaAs/Al}} = \frac{C_{\text{tot}}}{C_C} (\delta_A - \frac{C_L}{C_{\text{tot}}} \delta_B) \quad (2)$$

with trilayer capacitance $C_C = 285$ fF and inductor capacitance $C_L = 37.5$ fF, as determined by analysis and simulation, and loss values shown in Table I. For a parallel plate capacitor, $F = 1$, so we can say $\delta_{\text{Al/GaAs/Al}} = \delta_{\text{TLS,Al/GaAs/Al}}^0$.

From Eq. 2, we determine that $\delta_{\text{Al/GaAs/Al}} = 7.2 \times 10^{-5}$, slightly higher than the resonator-induced TLS loss for device A, $\delta_A = (6.4 \pm 0.2) \times 10^{-5}$, verifying that the TLS loss of device A is dominated by the Al/GaAs/Al trilayer. These values agree within a factor of two with bulk GaAs loss measurements.¹³

For a target qubit lifetime of 50 to 100 μs , losses must fall within the mid- 10^{-7} range. Thus, the measured loss

in this materials set is too high for superconducting qubit applications. Power-independent and TLS losses may be lower in other epitaxial trilayers such as Al/Si/Al and Al/Ge/Al.

IV. CONCLUSION AND NEXT STEPS

Due to the presence of significant power-independent loss in thin epitaxial Al/GaAs/Al trilayers, GaAs can be ruled out as a promising dielectric material for superconducting quantum computing applications unless mitigation methods are implemented. In the future, similar growth, fabrication and measurement techniques could be applied to other promising, non-piezoelectric materials sets such as epi-Al/Si/Al trilayers, and could yield substantial performance enhancement.

DATA AVAILABILITY

The data that support the findings of this study are openly available in Boulder-Cryogenic-Quantum-Testbed/data at <http://doi.org/10.5281/zenodo.4025406>.

ACKNOWLEDGMENTS

We wish to acknowledge the partial support of the Army Research Office, Google, and the NIST Quantum Initiative.

¹C. R. H. McRae, H. Wang, J. Gao, M. Vissers, T. Brecht, A. Dunsworth, D. Pappas, and J. Mutus, (2020), arXiv:2006.04718.

- ²S. Oh, K. Cicak, R. McDermott, K. B. Cooper, K. D. Osborn, R. W. Simmonds, M. Steffen, J. M. Martinis, and D. P. Pappas, *Supercond. Sci. Tech.* **18**, 1396 (2005).
- ³Y. Nakamura, H. Terai, K. Inomata, T. Yamamoto, W. Qiu, and Z. Wang, *Appl. Phys. Lett.* **99**, 212502 (2011), <https://doi.org/10.1063/1.3663539>.
- ⁴C. Müller, J. H. Cole, and J. Lisenfeld, *Rep. Prog. Phys.* **82**, 124501 (2019).
- ⁵A. Megrant, C. Neill, R. Barends, B. Chiaro, Y. Chen, L. Feigl, J. Kelly, E. Lucero, M. Mariantoni, P. J. O'Malley, *et al.*, *Appl. Phys. Lett.* **100**, 113510 (2012).
- ⁶C. J. Richardson, N. P. Siwak, J. Hackley, Z. K. Keane, J. E. Robinson, B. Arey, I. Arslan, and B. S. Palmer, *Supercond. Sci. Tech.* **29**, 064003 (2016).
- ⁷R. Zhao, S. Park, T. Zhao, M. Bal, C. R. H. McRae, J. Long, and D. P. Pappas, (2020), [arXiv:2008.07652](https://arxiv.org/abs/2008.07652).
- ⁸A. Y. Cho and P. D. Dernier, *Jour. Appl. Phys.* **49**, 3328 (1978), <https://doi.org/10.1063/1.325286>.
- ⁹P. M. Petroff, L. C. Feldman, A. Y. Cho, and R. S. Williams, *Jour. Appl. Phys.* **52**, 7317 (1981), <https://doi.org/10.1063/1.328722>.
- ¹⁰R. Ludeke and G. Landgren, *J. Vac. Sci. Technol.* **19**, 667 (1981), <https://doi.org/10.1116/1.571082>.
- ¹¹S. Pilkington and M. Missous, *J. Cryst. Growth* **196**, 1 (1999).
- ¹²A. McFadden, A. Goswami, M. Seas, C. R. H. McRae, R. Zhao, D. P. Pappas, and C. J. Palmstrøm, (2020), [arXiv:2007.10484](https://arxiv.org/abs/2007.10484).
- ¹³M. Scigliuzzo, L. E. Bruhat, A. Bengtsson, J. Burnett, A. F. Roudsari, and P. Delsing, *New J. Phys.* **22**, 053027 (2020).
- ¹⁴Certain commercial equipment, instruments, and materials are identified in this paper to foster understanding. Such identification does not imply recommendation or endorsement by the National Institute of Standards and Technology, nor does it imply that the materials or equipment identified are necessarily the best available for the purpose.
- ¹⁵C. R. H. McRae, R. E. Lake, J. L. Long, M. Bal, X. Wu, B. Jugdersuren, T. H. Metcalf, X. Liu, and D. P. Pappas, *Appl. Phys. Lett.* **116**, 194003 (2020).
- ¹⁶D. P. Pappas, M. R. Vissers, D. S. Wisbey, J. S. Kline, and J. Gao, *IEEE Trans. Appl. Supercond.* **21**, 871 (2011).
- ¹⁷M. Khalil, M. Stoutimore, F. Wellstood, and K. Osborn, *J. Appl. Phys.* **111**, 054510 (2012).
- ¹⁸<https://github.com/Boulder-Cryogenic-Quantum-Testbed/>.
- ¹⁹J. Burnett, A. Bengtsson, D. Niepce, and J. Bylander, *IOP Conf. Series: Journal of Physics: Conf. Series* **969**, 012131 (2018).